frontiers | Frontiers in Metals and Alloys

TYPE Original Research
PUBLISHED 26 September 2023
DOI 10.3389/ftmal.2023.1258941

OPEN ACCESS

EDITED BY
Mariah Hahn,
Rensselaer Polytechnic Institute,
United States

REVIEWED BY
Kaveh Rahmani,
Bu-Ali Sina University, Iran
Feng Huang,
Wuhan University of Science and Technology, China

*CORRESPONDENCE
M. A. Lira-Martínez,
manuel.lira@uacj.mx
C. Gaona-Tiburcio,
citlalli.gaona@gmail.com

RECEIVED 14 July 2023
ACCEPTED 30 August 2023
PUBLISHED 26 September 2023

CITATION
Jáquez-Muñoz JM, Castrejon AN, Lira-Martínez MA, Maldonado-Bandala E, Cabral-Miramontes J, Lara-Banda M, Estupiñán-López F, Nieves-Mendoza D, Gaona-Tiburcio C and Almeraya-Calderón F (2023), Corrosion behavior of aluminum-carbon fiber/epoxy sandwich composite exposed on NaCl solution.
Front. Met. Alloy 2:1258941.
doi: 10.3389/ftmal.2023.1258941

Corrosion behavior of aluminum-carbon fiber/epoxy sandwich composite exposed on NaCl solution

J. M. Jáquez-Muñoz[1,2], A. N. Castrejon[1], M. A. Lira-Martínez[1]*, E. Maldonado-Bandala[3], J. Cabral-Miramontes[2], M. Lara-Banda[2], F. Estupiñán-López[2], D. Nieves-Mendoza[3], C. Gaona-Tiburcio[2]* and F. Almeraya-Calderón[2]

[1]Departamento de Ingeniería Industrial y Manufactura, Instituto de Ingeniería y Tecnología, Universidad Autónoma de Ciudad Juárez, Ciudad Juárez, Mexico, [2]Facultad de Ingeniería Mecánica y Eléctrica, Centro de Investigación e Innovación en Ingeniería Aeronáutica (CIIIA), Universidad Autónoma de Nuevo León, San Nicolás de los Garza, Mexico, [3]Facultad de Ingeniería Civil—Xalapa, Universidad Veracruzana, Xalapa, Mexico

For years, the aeronautical industry has employed different types of materials to satisfy its high-performance requirements. Fiber-metal laminates are used due to their combination of lighter weight and the high mechanical properties of reinforced metal and carbon. We therefore made two different composites of laminate-metal and laminate-metal-laminate of carbon fiber-reinforced polymer and aluminum with an ALCLAD layer. The samples were characterized by salt fog (0, 48, and 96 h) at 5 wt% NaCl and electrochemical impedance spectroscopy (EIS) with an electrolyte of 3.5 wt% NaCl. All samples were studied by electron scanning microscopy (SEM). The results demonstrated that the samples of laminate-metal-laminate presented an adsorption process after 0 and 48 h of salt fog exposition; meanwhile, the samples of laminate-metal showed a capacitive behavior for all the samples; however, corrosion resistance decreased when the salt fog exposition time increased.

KEYWORDS

composite materials, fiber metal laminates, CFRP, CARALL, electrochemical impedance spectroscopy, SEM

1 Introduction

The aircraft industry requires correct material selection in parameters such as cost, manufacturing, maintenance, and properties. One alternative to conventional materials is composite materials due to their weight reduction. Airbus has begun to use GLARE (a laminate of glass fiber S2 and aluminum) for the A380 to increase the elastic module. However, glass fiber (GF) is not as resistant as carbon fiber; therefore, researchers have investigated the use of carbon fiber-reinforced polymer (CFRP) as an option for GF (Sinmazçelik et al., 2011; Wang et al., 2020; Hynes et al., 2022).

The combination of CFRP with aluminum laminate (Al-FRML) is called CARALL. Different researchers have studied the properties of CARALL, agreeing that it has good mechanical properties, such as high ultimate tensile strength, fracture toughness, fatigue, and impact resistance (Hamill et al., 2018a).

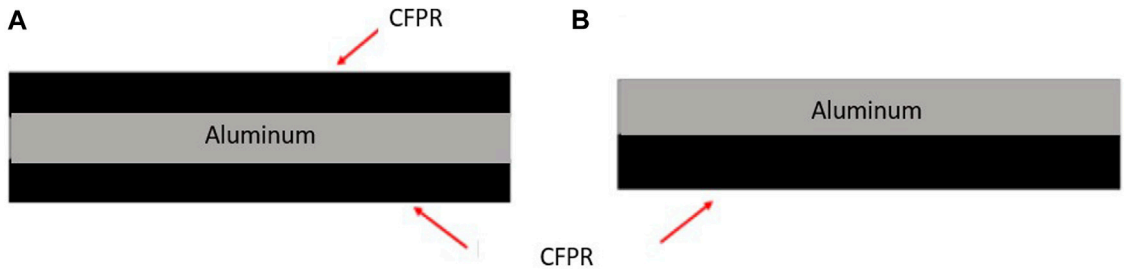

FIGURE 1
Schematic of experiment.

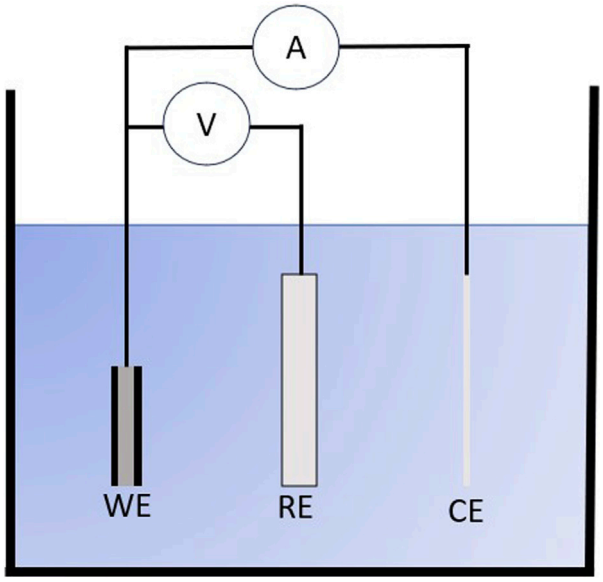

FIGURE 2
Schematic of corrosión test.

Nerveless, CARALL is not common because the difference between electrochemical potentials generates galvanic corrosion. The cathode is the CFRP due to the carbon fiber, and the aluminum (or almost any metal) is the anode. This characteristic increases the corrosion rate of material and is the biggest problem with CARALL (Sinmazçelik et al., 2011; Wu et al., 2021).

The aeronautical industry is the principal consumer of this type of material but must solve the problems of galvanic corrosion and thermal difference. In addition, anodized Al is employed as an effective coating to avoid galvanic corrosion (Twite and Bierwagen, 1998; Vogelesang and Vlot, 2000). The Delft University of Technology was one of the first to investigate CARALL's characteristics and found that galvanic corrosion occurs in the system. Galvanic corrosion in laminate materials has been reported when carbon fiber begins electrical contact with the metal and the electrolyte (Tavakkolizadeh and Saadatmanesh, 2001). Furthermore, galvanic corrosion reduces when carbon fiber is coated by epoxy and exists as an ALCLAD layer (Asundi and Choi, 1997).

Setvati and Mustaffa (2018) found that thin metal is important for increasing the corrosion resistance of fiber metal laminates. The use of aluminum sheets of 0.3–0.5 mm presents a lower corrosion rate than sheets of 2–4 mm. This result can be related to a decrease in anode area.

Various studies have analyzed the behavior of anodized aluminum and some Ti alloys with CFRP, finding that galvanic corrosion occurs to a lesser degree, but does occur. The exposition of CARALL in the marine environment over 6 months found galvanic corrosion in zones of the couple. Vermeeren (1991) found that one option is to isolate aluminum from carbon fiber, which can be achieved by epoxy or an anodized process.

Wu and Yang (2005) found that, when CARALL was immersed in solution, corrosion reduced. This is also related to water adsorption; however, corrosion susceptibility calculated by potentiodynamic polarization shows that the corrosion of CARALL was greater than for aluminum alloy uncoated in NaCl at 3.5%. The samples showed the characteristic of the intergranular system, attributed to the pitting process, where the pitting breaks the boundaries.

Pan et al. (2017) concluded that separating the metal from the CFRP is necessary to reduce the corrosion rate and galvanic corrosion. In addition, an increase in pH is an important factor in the corrosion rate of these materials. CFRP/metal in NaCl at 3.5 wt% presented corrosion and delamination between CFRP and metal, breaking the adhesive composite metal (Pan et al., 2017). Furthermore, the products formed did not protect the material.

Setvati and Mustaffa (2018) demonstrated that CFRP with metals does not present uniform corrosion, but only corrosion in preferential zones when exposed to the material in NaCl at 0.6 M. Some authors have thus employed a fiber made of a hybrid of carbon and glass; they reported that galvanic corrosion was eliminated.

CFRP cannot be corroded, but it can degrade in a corrosive environment. Wu et al. (2014) concluded that a glass and carbon fiber composite can be attacked by salt and water solution, changing the composition and degrading the composite matrix. Pan et al. (2017) found that the galvanic corrosion rate is directly related to epoxy coating thickness. In addition, when pH is higher than 7, they recommend avoiding using a matrix with hydrolyzable links due to the hydroxide evolution. Vinayagamoorthy et al. (2018) recommended consideration of environmental conditions such as temperature, humidity, and the

10.3389/ftmal.2023.1258941

TABLE 1 Parameters obtained by Zview simulation.

Sample	Rs ($\Omega \cdot cm^2$)	R_{ct} ($\Omega \cdot cm^2$)	CPE-T (F/cm^2)	n	R_2 ($\Omega \cdot cm^2$)	CPE-T2 (F/cm^2)	n	L ($\Omega \cdot s \cdot cm^2$)	X^2
A1	0.91 ± 0.04	319 ± 5.3	$5.11 \times 10^{-4} \pm 2 \times 10^{-5}$	0.8 ± 0.1	171 ± 15.6			2066 ± 102	0.01
A2	2.75 ± 0.30	415 ± 10.2	$1.48 \times 10^{-3} \pm 1 \times 10^{-5}$	0.6 ± 0.05	565 ± 25.4			456 ± 23	0.02
A3	0.88 ± 0.16	108 ± 1.6	$5.37 \times 10^{-3} \pm 5 \times 10^{-5}$	0.7 ± 0.03	59 ± 5.4	$4.16 \times 10^{-1} \pm 5 \times 10^{-2}$	1 ± 0.01		0.01
B1	0.67 ± 0.31	330 ± 15.6	$2.89 \times 10^{-3} \pm 2 \times 10^{-5}$	0.7 ± 0.01	771 ± 17.6	$2.54 \times 10^{-1} \pm 3 \times 10^{-2}$	1 ± 0.02		0.02
B2	1.55 ± 0.45	368 ± 17.8	$2.36 \times 10^{-3} \pm 3 \times 10^{-5}$	0.7 ± 0.04	214 ± 13.2	$1.13 \times 10^{-1} \pm 8 \times 10^{-2}$	1 ± 0.01		0.03
B3	0.94 ± 0.03	6 ± 3.5	$5.86 \times 10^{-4} \pm 4 \times 10^{-5}$	0.8 ± 0.01	551 ± 10.8	$1.68 \times 10^{-3} \pm 2 \times 10^{-4}$	0.7 ± 0.01		0.02

chemical conditions of the medium (acidic), as well as applying a coating to the fiber-reinforcement to reduce the degradation of the composite. Due to the angle of CFRP influence, it has been found that samples with an angle of 30° present higher SCC in acidic media.

Wang et al. (2007) and Wang et al. (2020) immersed CARALL with different treatments (anodized and sol-gel coatings). The samples with coatings did not present corrosion after 300 and 900 h, reducing corrosion problems. Furthermore, CARALL is fabricated by a conventional curing process. When exposed to an electrolyte, there is electrical conductivity between the composite/metal interface. To protect the aluminum-metal interface, some recommend the use of thermoplastics, epoxy resin, and coatings on aluminum surfaces (Habazaki et al., 2007; Hamill et al., 2018; Mukesh and Rajesh Jesudoss Hynes, 2019). Anodized samples reduce the corrosion rate of materials.

This work aims to study the corrosion kinetic of CFRP-Aluminum 7075 laminate with ALCLAD coating. The carbon fiber used is T300 in the epoxy matrix. The samples were exposed to salt fog for 96 h based on ASTM B-117. The electrochemical characterization was achieved with samples at 0, 48, and 96 h of salt fog by electrochemical impedance spectroscopy (EIS). While the behavior of these composites employing potendiodynamic polarization, EIS, or salt fog has been previously researched, salt fog and an electrochemical technique have rarely been mixed. This research relates salt fog with the electrochemical characterization of composites and indicates the changes of the electrochemical behavior of composites after different exposure hours to salt fog.

2 Materials and methods

2.1 Materials and CFRP fabrication

The materials employed in this research were Al-7075 sheets of 3 mm thickness; these were used with ALCLAD of receiving conditions. For the fabrication of CFRP, a specialized epoxy matrix (EP-1 Hetzen) for the aircraft industry was used, and the catalyzer application was 5% epoxy by weight. The infusion was relized by vaccum, the carbon fiber used was TORAYCA T300 unidirectional. The samples were made by vacuum process at 38 °C. Two types of sample were prepared, with one and two CFRP layers (Figure 1). The time between the samples being made (vacuum) and the corrosion test was 1 week.

2.2 Corrosion testing

The salt fog used was Q-Fog SSP LF 8810, and the salt spray test was performed based on ASTM B-117 for 96 h (ASTM International, 2003). The electrochemical characterization was performed in a conventional three-electrode cell (work electrode, saturated calomel reference electrode, and platinum counter electrode) using EIS from 100 kHz to 10 mHz based on ASTM G-106 in 3.5 wt% NaCl electrolyte (ASTM Norma G 106, 1999). The samples of EIS experiments were the CARALL after 0, 48, and 96 h of salt fog. The EIS was simulated using the Zview program. The experiments were done in triplicate. The standard deviation of each

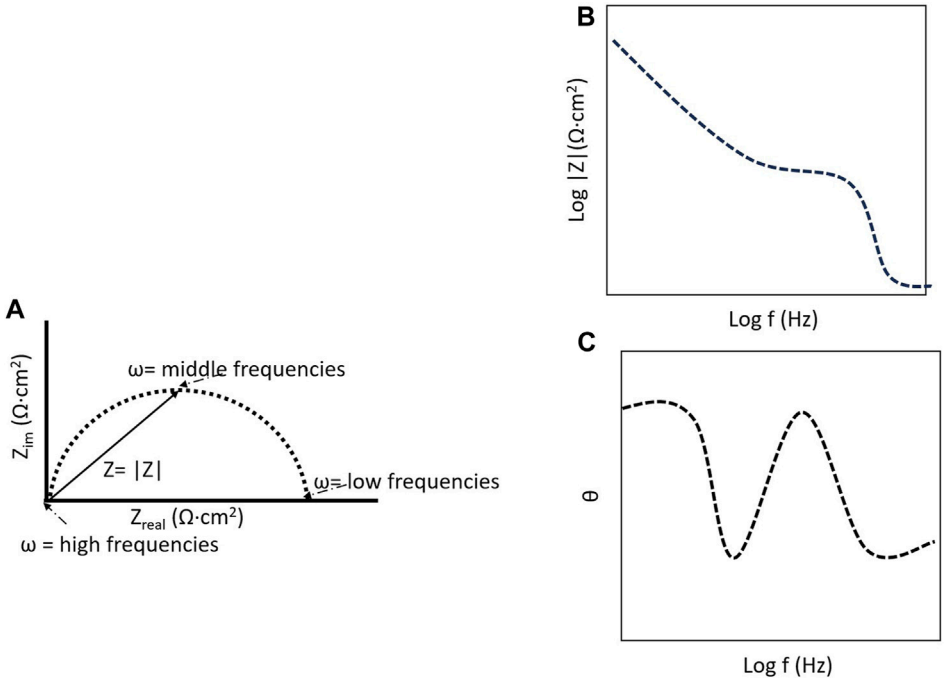

FIGURE 3
(A) Nyquist diagram, **(B)** Bode diagram frequency vs. Impedance magnitude, **(C)** frequency vs. Phase angle.

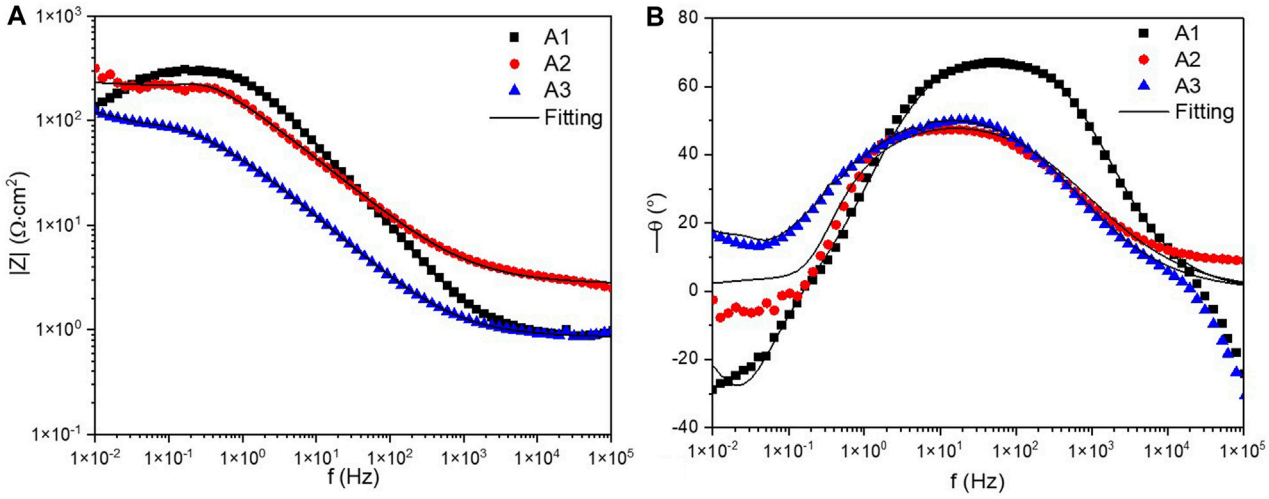

FIGURE 4
Nyquist Diagrams of samples A exposed in NaCl at 3.5 % wt.

result of the EIS simulation was added to consider the variation between each experiment and its simulation.

2.3 SEM-EDS analysis

Samples were sectioned and analyzed using scanning electron microscopy (SEM, JEOL-JSM-5610 LV) operating at 20 kV. The surface characterization was realized by backscattered electrons (BSE) and secondary electron (SE) detectors.

3 Results and discussion

3.1 Electrochemical impedance spectroscopy

Figure 2 shows the samples' behavior when exposed to 3.5 wt% NaCl solution after exposure to salt fog. The Nyquist diagram shows that the samples exposed during 0 and 48 h presented inductive behavior at low frequencies. This behavior is related to the adsorption process in the surface. It was evident that the

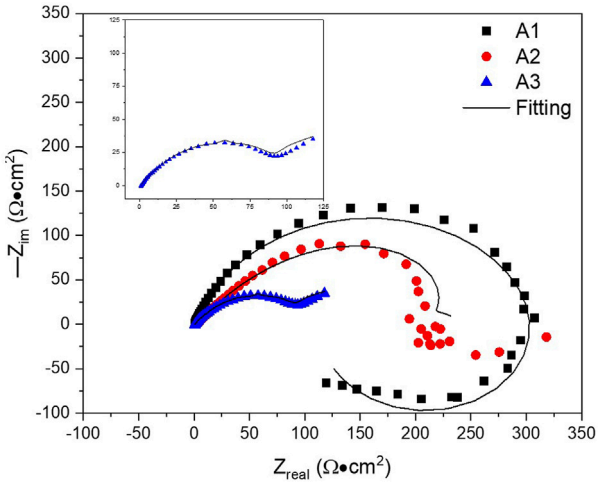

FIGURE 5
Bode Diagrams **(A)** |Z| vs. Frequency and **(B)** angle of phase vs. frequency of samples A exposed in NaCl at 3.5 % wt.

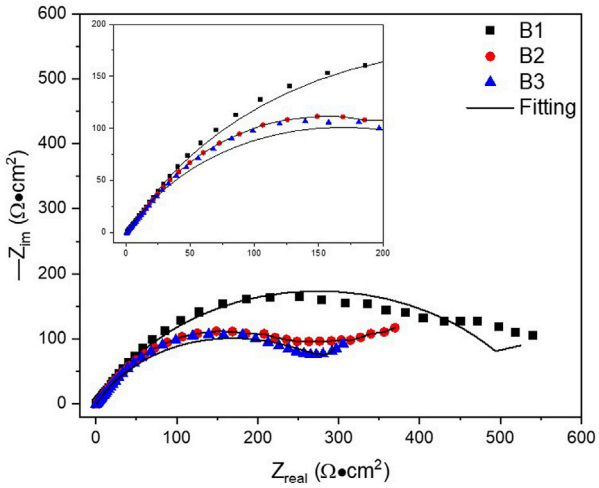

FIGURE 6
Nyquist Diagrams of samples B exposed in NaCl at 3.5 % wt.

resistance of samples decreased when the hours of exposure in the salt fog increased (Table 1). The R_{ct} decreased from 319 to 108 Ω cm^2 for A1 to A3 samples, indicating a lower charge transference resistance between the samples exposed to the saline environment. The value of the CPE increased at 48 and 96 h, indicating that ionic charges increased due to material degradation. Furthermore, the value of *n* decreased when the exposure hours increased.

In the inductive behavior, it is notable that the inductivity value reduced from 2066 to 456 Ω s cm^2 at 0 and 48 h of exposure. After 96 h exposure to salt fog, the sample lost its inductive behavior and had a pure capacitive behavior, with an *n* value of 1. The decrease in corrosion resistance is attributed to the delamination of composite and aluminum, which induces galvanic and intergranular corrosion (Ostapiuk and Bieniaś, 2021). The main problem is resin degradation that provokes the galvanic coupling between carbon fiber and ALCLAD. Various authors have related the inductive loop with a weakening of the protective layer of aluminum (Cao et al., 1989; Keddam et al., 1997; Li et al., 2009). The justification for using an inductor for this behavior and in the equivalent circuit (Figure 6) is the dissolution of the ALCLAD layer at low frequency (Shkirskiy et al., 2015). Furthermore, the adsorption that occurs is of the dissolute species (Kissi et al., 2006).

When salt fog time increases, the inductance is reduced and has a capacitive behavior at medium and low frequencies, which is related to the new surface characteristics due to the dissolution of the oxide layer (Conde and De Damborenea, 1998; 2000; Li et al., 2009). When the exposure time to some media increases, the process of corrosion exfoliation is higher, so the two arcs are present. In addition, the capacitive arc is related to the material's relaxation process and dielectric properties (Aberd et al., 2001; Bouklah et al., 2005). The transformation from an inductive to a capacitive process is associated with a more intense corrosion process. Furthermore, some relate the inductive loop with the corrosion process (Mansfeld, 1993; Zhang and Cheng, 2009; Jingling et al., 2010). For these samples, the inductive loop is associated with an adsorption process that weakens the ALCLAD, making it susceptible to pitting.

The table values were obtained using Eqs. 1–3. Eq. 1 correspond to a capacitance system, where *i* is the current, *w* is the frequency, and *C* is the capacitance. Eq. 2 corresponds to the constant phase element, where the *α* exponent corresponds to the *n* value, and *q* is the charge. Eq. 3 shows the calculated inductance, where *L* is the induction. Figure 3 shows examples of the diagrams obtained by EIS.

$$\boldsymbol{Z_c(\omega) = \frac{1}{i\omega C}} \tag{1}$$

$$\boldsymbol{Z_{CPE}(\omega) = \frac{1}{(i\omega)^{\alpha_{dl}} Q^{dl}}} \tag{2}$$

$$\boldsymbol{Z_L(\omega) = i\omega L} \tag{3}$$

Figure 4 shows the Bode diagrams of Sample A exposed in NaCl at 3.5% wt. The |Z| vs. frequency diagram shows that Sample A3 presented lower impedance values even at high and low frequencies. In addition, the angle phase diagram shows how two processes exist in the system, with the change at low frequencies from 100 to 10 mHz. The change in behavior from inductive to capacitive is related to the transition from species' adsorption to the transference of electrons and higher material degradation. The first arc of Figure 5 (high frequency) is related to the capacitance resistance of the epoxy-carbon fiber resistance (it is also the first semicircle of Figure 2) and is also related to the charge transference between the aluminum and the electrolyte at low frequencies (Pan et al., 2018).

Figure 6 shows the Nyquist diagrams of Sample B exposed in NaCl at 3.5% wt. In this case, all the samples present capacitive behavior. Sample B1 presented the higher total resistance, as shown by the Nyquist diagram, and the value of the charge transference resistance is like B2, with 330 and 368 Ω cm^2; however, the value of R_{ct} of B3 is of 3 Ω cm^2, indicating a low resistance to the charge transference due to the material's degradation. The value of *n* is 0.7 for B1 and B2, indicating similar behavior. In the second layer's behavior, B1 presented the higher resistance, 771 Ω cm^2; meanwhile, sample B3 showed a low capacitance value of 1.68×10^{-3} F/cm^2, with a *n* of 0.7.

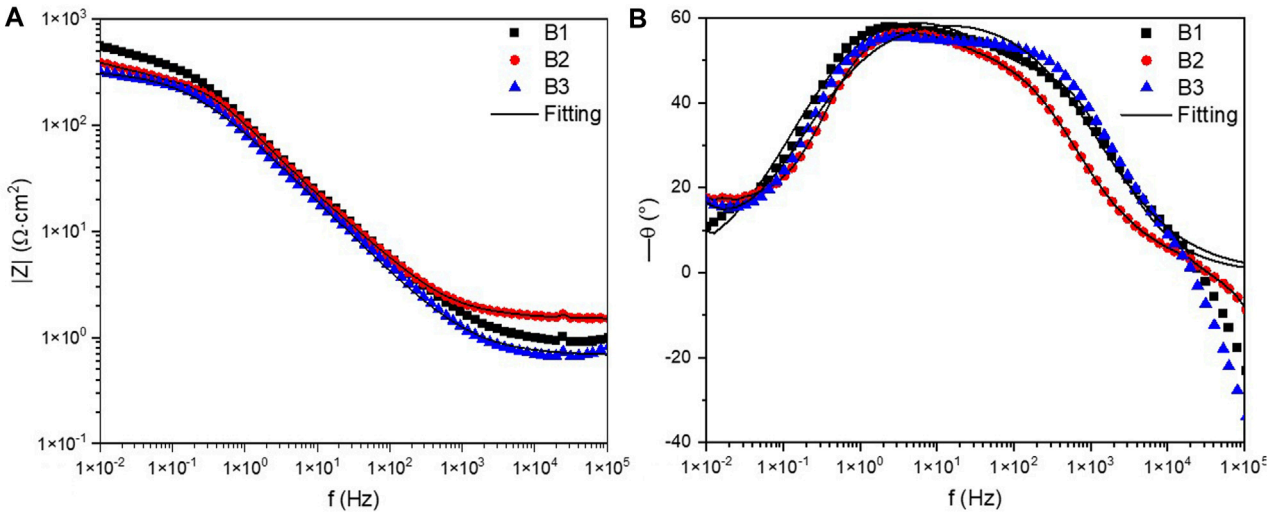

FIGURE 7
Bode Diagrams **(A)** |Z| vs. Frequency and **(B)** angle of phase vs. frequency of samples B exposed in NaCl at 3.5 % wt.

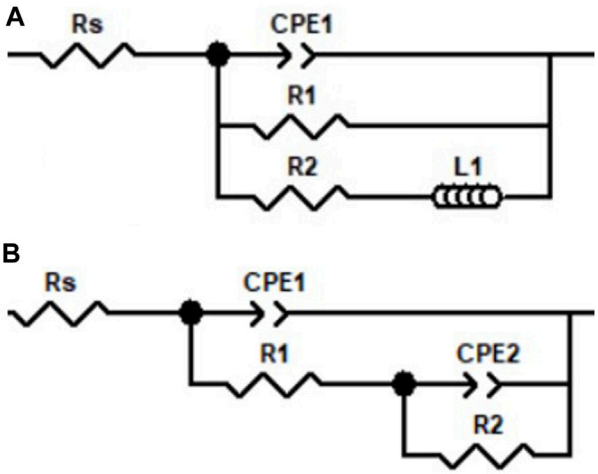

FIGURE 8
Equivalent circuits for **(A)** A1 and A2, and **(B)** A3. B1–B3.

The decrease of R_{ct} corresponds with micropore defects of resin. When the R_{ct} increase is related to the deposition of corrosion residues in the first layer, however, it provokes a powerful Cl^- penetration in the next layer, reducing corrosion resistance (Deyab et al., 2017). Therefore, the second layer in all the B samples is associated with capacitance, not another element. After 96 h of salt fog exposure, Sample B3 showed a reduction in *n* value to 0.7, indicating that the charge distribution is heterogeneous, but the process changes from a uniform to a possible diffusion (Eltai et al., 2012; Vakili et al., 2015; Refait et al., 2018). This is related to blocked diffusion (Bisquert et al., 1998). Block diffusion considered the decrease of the second arc when exposition time increases; that behavior is related to a decrease in the dielectric properties of the material and more corrosion exposition (Sherif et al., 2019). That behavior can relate to the oxide/hydroxide layer when hydrogen evolution occurs (Curioni et al., 2015).

Figure 7 shows the Bode diagrams of B. For the Z magnitude diagram from Figure 4A at low frequencies, Sample B1 presented the highest impedance, and B3 showed the lower values. In the angle phase diagram (Figure 4B), it is evident how all the samples presented two processes. The second process occurs at low frequencies.

Table 1 shows the results from EIS parameters obtained by Zview simulation. After 96 h of exposition, all the samples presented a decrease the R_{ct} resistance, with values of 108 and 6 Ω cm^2 for A3 and B3. The samples covered as a sandwich presented a higher corrosion resistance, including R_{ct}, R_2, and the resistance generated by the inductance. However, the resistance after 96 h is higher for the B3 sample. The values of CPE from the second part of the circuit presented an increase in their values from $\times10^{-3}$ to $\times10^{-1}$ F/cm^2, and relate that behavior to an increase in the ionic transport and more facilities of ionic transport.

Figure 8 shows the two equivalent circuits obtained. Samples A1 and A2 presented an inductive behavior, so the circuit presented an inductor. The rest of the samples showed a double-layer behavior.

Figure 9 shows the corrosion mechanism that occurs on composite. The electrolyte ions (Cl^- and OH^-) are present on the surface, and the CFRP matrix begins degradation. After degradation, the ions are deposited on the attacked surface, producing adsorption until the CFRP further degrades by exposure and Cl penetration. The capacitive behavior at low frequencies occurs due to the Cl^- ion penetration; consequently, after 96 h exposure, the Nyquist diagram changes from inductive to capacitive behavior. It is important to mention that the particles of C act as a cathode and are very dangerous for aluminum exposure. However, ALCLAD helps reduce the effects of C and Cl^-.

3.2 SEM-EDS results

Figure 10 shows the SEM-EDS analysis of the samples transversal section A. Sample A1 (Figure 10A), which was

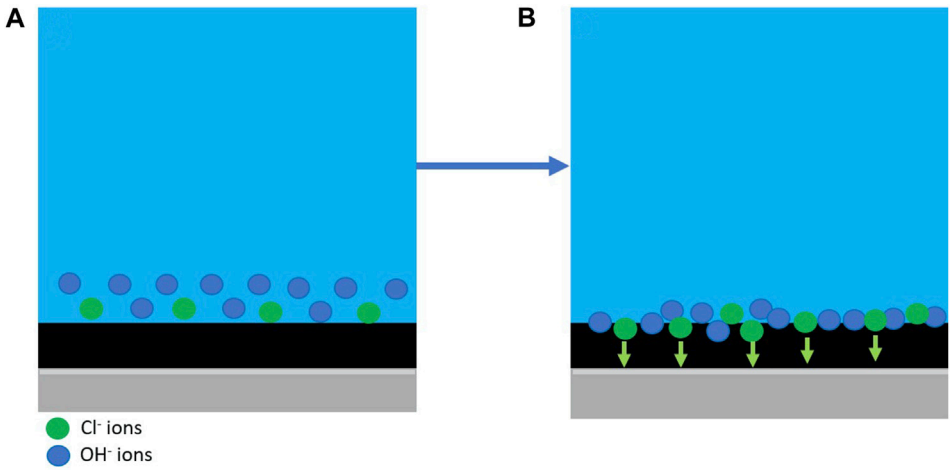

FIGURE 9
Corrosion mechanism. **(A)** first interaction of composite with electrolyte. **(B)** interaction after CFRP matrix degradation.

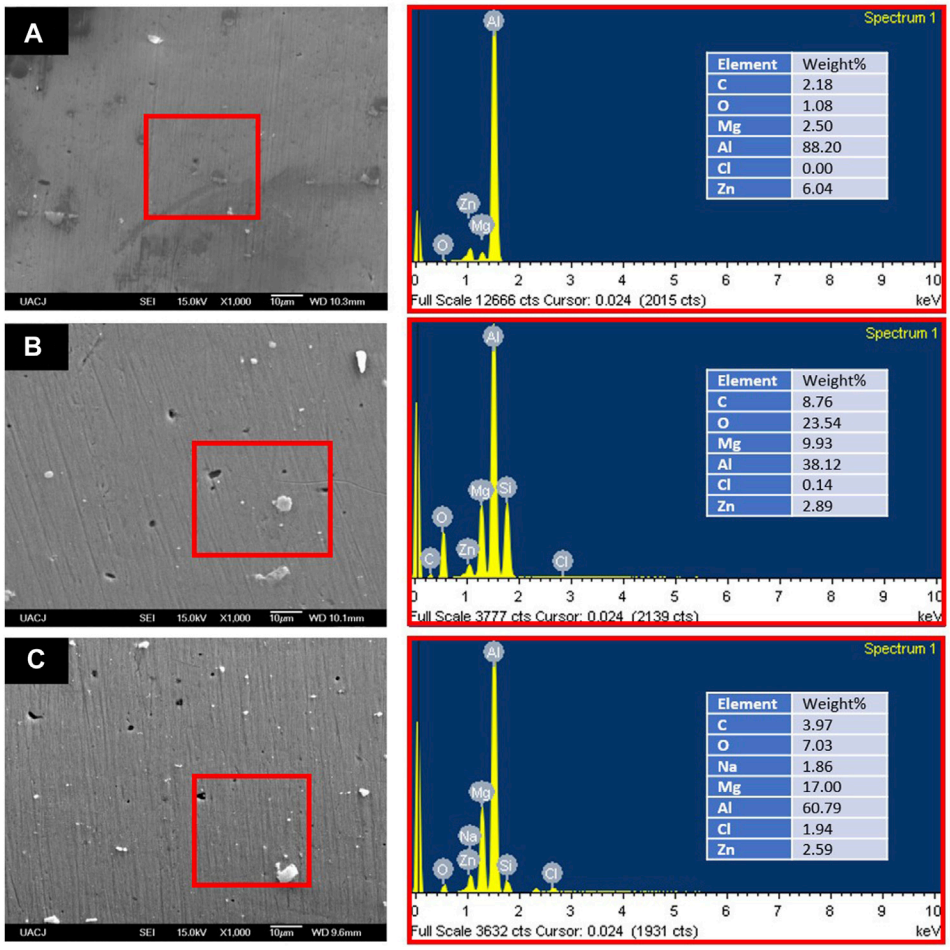

FIGURE 10
SEM-EDS **(A)** A1, **(B)** A2, and **(C)** A3 at 1000 X.

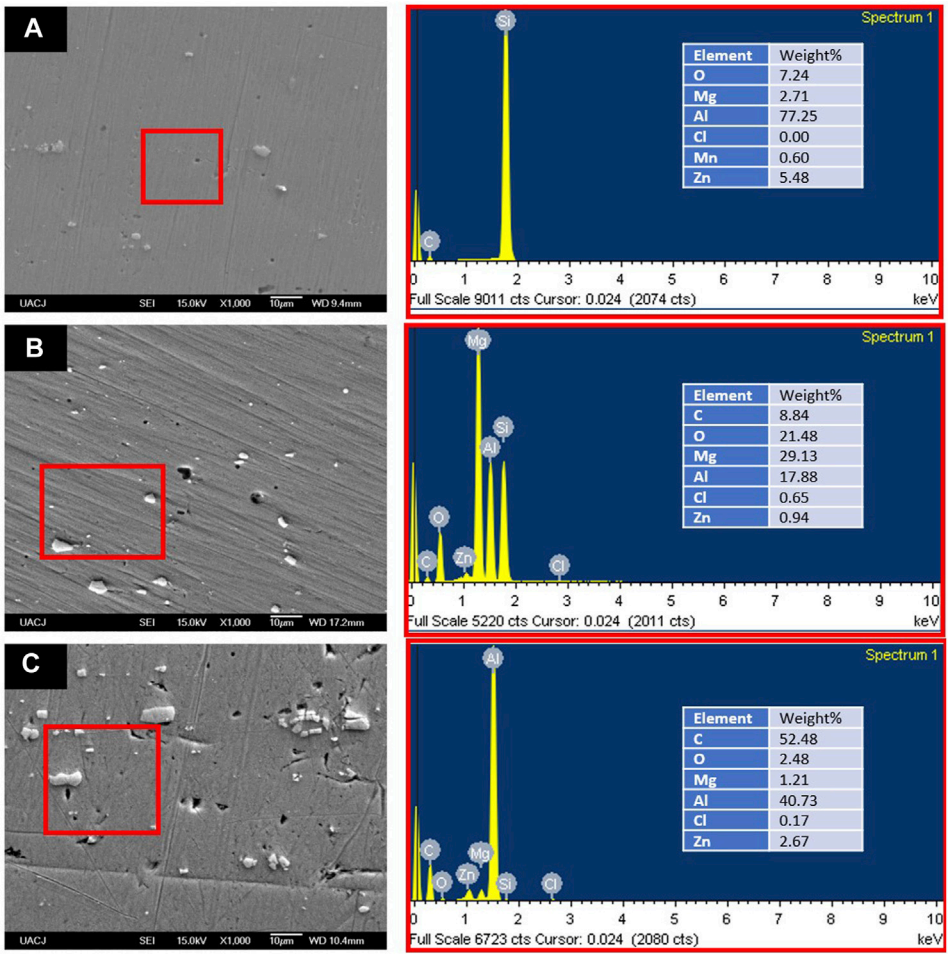

FIGURE 11
SEM-EDS of **(A)** B1, **(B)** B2, and **(C)** B3 at 1000 X.

exposed for 0 h to salt fog and was characterized by EIS at 3.5 wt% NaCl, presented a low presence of O, but Cl was not present, indicating that Cl did not cross that section. After 48 h in salt fog and characterized by EIS, the presence of O and Cl was detected, suggesting that, when exposure hours increase, Cl penetrated the material (Figure 10B). That behavior is shown in Sample A3 in Figure 10C; the presence of Cl increases, and Na is presented. It is important to note that C is present in the three samples; this behavior can be related to a dissociation of epoxy that exposes the carbon fiber and facilities the attack of Cl^- ions.

The pitting occurring in the aluminum surface has the morphology of peripheral pitting due to the action of cathodic sites (carbon fiber) on the surface, causing the dissolution of the matrix and its periphery. The process consists of individual attacks and nucleation (0 and 48 h with EIS characterization) for micro-attacks in the subsurface (48 and 96 h) during exposure to corrosive environments (Hamill et al., 2018). Birbilis et al. (2006) showed that pitting could be classified into two categories: peripheral that appears as a ring around the inclusions, and when the pit contains residual particles, usually dippers. In this case, adoption processes at 0 and 48 h can be related to a displacement of Cl^- adsorption due to decreased cathode sites. The porosity of ALCLAD that permits the Cl^- alumina hydration can block penetration; for that reason, the EDS analysis showed a low presence of Cl in the transversal zone; however, it showed the presence of C acting as the cathode, which can provoke intergranular corrosion.

Figure 11 shows the SEM-EDS analysis of samples transversal section B. Figure 11A shows the results of Sample B1, which did not present pitting and Cl presence. Figure 11B shows Sample B2 after 48 h of salt fog exposition and EIS characterization. In this sample, O, C, and Cl increased; this result is associated with CFRP degradation, which induces corrosion. Sample B3 in Figure 11C shows an increase in pitting of the transversal section, and the EDS shows a high presence of C; this behavior is related to a high degradation of the CFRP, which exposes the material to Cl and C and increases the material's degradation.

4 Conclusion

- When the metal-laminate composite was realized as a sandwich structure (CFRP-Al-CFRP), the samples presented an inductive behavior in the EIS characterization, indicating

that the electrolyte ions will be adsorbed in the CFRP surface during the first exposure hours.
- Sample A3 presented the lowest impedance, with 167 Ω cm^2 (R_{ct} + R_2) compared to the other samples.
- Sample B3 showed the lowest R_{ct} value, 6 Ω cm^2, indicating a low resistance to charge transference.
- The samples of B were the most degraded in the SEM analysis, with more corrosion elements present and more pitting, indicating that the sandwich structure exhibits better behavior against corrosion.
- Use of laminate-metal-laminate provokes the adsorption process in the laminate surface because the CFPR helps the process. On the other hand, using a laminate-metal composite generates a capacitive reaction due to the exposure of Al to the electrolyte and reduces the corrosion resistance.
- The electrolyte's exposure provoked the break of hydrogen and oxygen chains, affecting the composite. Therefore, the EDS analysis presented C, Cl, and Na elements.
- The use of aluminum with an ALCLAD coating helped reduce the kinetic corrosion of the composite, in comparison with other research that used aluminum without coating or with an organic coating; in addition, the ALCLAD layer helps reduce the galvanic coupling of Al and CFRP. However, the epoxy matrix degraded easily and attacked the material surface with C and Cl. Furthermore, the thickness of aluminum helps deteriorate the composite faster because it is a large anode.
- A CFRP sandwich must be applied to increase the composite's corrosion resistance, avoiding the exposition of Al to electrolyte media, even if it has the ALCLAD coating.

Data availability statement

The raw data supporting the conclusions of this article will be made available by the authors, without undue reservation.

Author contributions

JJ-M: conceptualization, data curation, formal analysis, investigation, methodology, project administration, writing–original draft, writing–review and editing. AC: conceptualization, investigation, writing–original draft. ML-M: writing–original draft. EM-B: writing–review and editing. JC-M: writing–review and editing. ML-B: writing–review and editing. FE-L: writing–review and editing. DN-M: writing–review and editing. CG-T: conceptualization, investigation, writing–original draft, writing–review and editing. FA-C: conceptualization, data curation, investigation, methodology, software, supervision, writing–original draft, writing–review and editing.

Funding

The authors declare that no financial support was received for the research, authorship, and/or publication of this article.

Acknowledgments

The authors acknowledge the Academic Body UANL—CA-316 "Deterioration and integrity of composite materials".

Conflict of interest

The authors declare that the research was conducted in the absence of any commercial or financial relationships that could be construed as a potential conflict of interest.

The authors declared that they were an editorial board member of Frontiers, at the time of submission. This had no impact on the peer review process and the final decision.

Publisher's note

References

Aberd, Y., Hammouti, B., Kertit, S., El Kacemi, K., and Mansri, A. (2001). Poly (4-vinylpuridine)(P4VP) as corrosion inhibitors. *Bull. Electrochem.* 17, 105.

ASTM International (2003) "Standard practice for operating salt spray (FOG) apparatus.," *Water*, 03, pp. 1–15. Available at: https://www.astm.org/b0117-19.html (Accessed: June 25, 2023).

ASTM Norma G 106 (1999). *Standard practice for verification of algorithm and equipment for electrochemical impedance measurements*. Astm, 1–11. Available at: https://www.astm.org/g0106-89r15.html (Accessed January 18, 2023).

Asundi, A., and Choi, A. Y. N. (1997). Fiber metal laminates: an advanced material for future aircraft. *J. Mater. Process. Technol.* 63 (1–3), 384–394. doi:10.1016/S0924-0136(96)02652-0

Birbilis, N., Cavanaugh, M. K., and Buchheit, R. G. (2006). Electrochemical behavior and localized corrosion associated with Al7Cu2Fe particles in aluminum alloy 7075-T651. *Corros. Sci.* 48 (12), 4202–4215. doi:10.1016/J.CORSCI.2006.02.007

Bisquert, J., Garcia-Belmonte, G., Bueno, P., Longo, E., and Bulhões, L. (1998). Impedance of constant phase element (CPE)-blocked diffusion in film electrodes. *J. Electroanal. Chem.* 452 (2), 229–234. doi:10.1016/S0022-0728(98)00115-6

Bouklah, M., Attayibat, A., Kertit, S., Ramdani, A., and Hammouti, B. (2005). A pyrazine derivative as corrosion inhibitor for steel in sulphuric acid solution. *Appl. Surf. Sci.* 242 (3–4), 399–406. doi:10.1016/J.APSUSC.2004.09.005

Cao, C. N., Wang, J., and Lin, H. C. (1989). EFFECT OF Cl ION ON THE IMPEDANCE OF PASSIVE-FILM-COVERED ELECTRODES. *J. Chin. Soc. Corros. Prot.* 9 (4), 261–270. Available at: https://www.jcscp.org/EN/abstract/abstract17387.shtml (Accessed July 14, 2023).

Conde, A., and De Damborenea, J. (1998). Electrochemical modelling of exfoliation corrosion behaviour of 8090 alloy. *Electrochimica Acta* 43 (8), 849–860. doi:10.1016/S0013-4686(97)00218-1

Conde, A., and De Damborenea, J. (2000). Evaluation of exfoliation susceptibility by means of the electrochemical impedance spectroscopy. *Corros. Sci.* 42 (8), 1363–1377. doi:10.1016/S0010-938X(00)00006-8

Curioni, M., Scenini, F., Monetta, T., and Bellucci, F. (2015). Correlation between electrochemical impedance measurements and corrosion rate of magnesium investigated by real-time hydrogen measurement and optical imaging. *Electrochimica Acta* 166, 372–384. doi:10.1016/J.ELECTACTA.2015.03.050

Deyab, M. A., Ouarsal, R., Al-Sabagh, A., Lachkar, M., and El Bali, B. (2017). Enhancement of corrosion protection performance of epoxy coating by introducing new hydrogenphosphate compound. *Prog. Org. Coatings* 107, 37–42. doi:10.1016/J.PORGCOAT.2017.03.014

Eltai, E. O., Scantlebury, J. D., and Koroleva, E. V. (2012). Protective properties of intact unpigmented epoxy coated mild steel under cathodic protection. *Prog. Org. Coatings* 73 (1), 8–13. doi:10.1016/J.PORGCOAT.2011.08.012

Habazaki, H., Onodera, T., Fushimi, K., Konno, H., and Toyotake, K. (2007). Spark anodizing of β-Ti alloy for wear-resistant coating. *Surf. Coatings Technol.* 201 (21), 8730–8737. doi:10.1016/J.SURFCOAT.2006.05.041

Hamill, L., Hofmann, D. C., and Nutt, S. (2018). Galvanic corrosion and mechanical behavior of fiber metal laminates of metallic glass and carbon fiber composites. *Adv. Eng. Mater.* 20 (2), 1700711. doi:10.1002/ADEM.201700711

Hynes, N. R. J., Vignesh, N. J., Barile, C., Velu, P. S., Baskaran, T., Jappes, J. T. W., et al. (2022). Green corrosion inhibition on carbon-fibre-reinforced aluminium laminate in NaCl using aerva lanata flower extract. *Polymers* 14 (9), 1700. doi:10.3390/POLYM14091700

Jingling, M. A., Jiuba, W., Gengxin, L., and Chunhua, X. (2010). The corrosion behaviour of Al–Zn–In–Mg–Ti alloy in NaCl solution. *Corros. Sci.* 52 (2), 534–539. doi:10.1016/J.CORSCI.2009.10.010

Keddam, M., Kuntz, C., Takenouti, H., Schustert, D., and Zuili, D. (1997). Exfoliation corrosion of aluminium alloys examined by electrode impedance. *Electrochimica Acta* 42 (1), 87–97. doi:10.1016/0013-4686(96)00170-3

Kissi, M., Bouklah, M., Hammouti, B., and Benkaddour, M. (2006). Establishment of equivalent circuits from electrochemical impedance spectroscopy study of corrosion inhibition of steel by pyrazine in sulphuric acidic solution. *Appl. Surf. Sci.* 252 (12), 4190–4197. doi:10.1016/J.APSUSC.2005.06.035

Li, J. F., Jia, Z. Q., Birbilis, N., and Cai, C. (2009). Exfoliation corrosion of 7150 Al alloy with various tempers and its electrochemical impedance spectroscopy in EXCO solution. *Mater. Corros.* 60 (6), 407–414. doi:10.1002/MACO.200805102

Mansfeld, F. (1993). Models for the impedance behavior of protective coatings and cases of localized corrosion. *Electrochimica Acta* 38 (14), 1891–1897. doi:10.1016/0013-4686(93)80311-M

Mukesh, A. M., and Rajesh Jesudoss Hynes, N. (2019). Corrosion behaviour of fibre metal laminates and control by inhibitors. *AIP Conf. Proc.* 2142 (1). doi:10.1063/1.5122400/725339

Ostapiuk, M., and Bieniaś, J. (2021). Corrosion resistance in NaCl environment of fiber metal laminates based on aluminum and titanium alloys with carbon and glass fibers. *Adv. Eng. Mater.* 23, 2001030. doi:10.1002/adem.202001030

Pan, Y., Wu, G., Huang, Z., Wu, X., Liu, Y., and Ye, H. (2017). Corrosion behaviour of carbon fibre reinforced polymer/magnesium alloy hybrid laminates. *Corros. Sci.* 115, 152–158. doi:10.1016/J.CORSCI.2016.11.022

Pan, L., Ding, W., Ma, W., Hu, J., Pang, X., Wang, F., et al. (2018). Galvanic corrosion protection and durability of polyaniline-reinforced epoxy adhesive for bond-riveted joints in AA5083/Cf/Epoxy laminates. *Mater. Des.* 160, 1106–1116. doi:10.1016/J.MATDES.2018.10.034

Refait, P., Grolleau, A. M., Jeannin, M., François, E., and Sabot, R. (2018). Corrosion of mild steel at the seawater/sediments interface: mechanisms and kinetics. *Corros. Sci.* 130, 76–84. doi:10.1016/J.CORSCI.2017.10.016

Setvati, M. R., and Mustaffa, Z. (2018). Rehabilitation of notched circular hollow sectional steel beam using CFRP patch. *Steel Compos. Struct.* 26 (2), 151–161. doi:10.12989/scs.2018.26.2.151

Sherif, E. S. M., Abdo, H. S., Latief, F. H., Alharthi, N. H., and Abedin, S. Z. E. (2019). Fabrication of Ti–Al–Cu new alloys by inductive sintering, characterization, and corrosion evaluation. *J. Mater. Res. Technol.* 8 (5), 4302–4311. doi:10.1016/J.JMRT.2019.07.040

Shkirskiy, V., King, A. D., Gharbi, O., Volovitch, P., Scully, J. R., Ogle, K., et al. (2015). Revisiting the electrochemical impedance spectroscopy of magnesium with online inductively coupled plasma atomic emission spectroscopy. *ChemPhysChem* 16 (3), 536–539. doi:10.1002/CPHC.201402666

Sinmazçelik, T., Avcu, E., Bora, M. Ö., and Çoban, O. (2011). A review: fibre metal laminates, background, bonding types and applied test methods. *Mater. Des.* 32 (7), 3671–3685. doi:10.1016/J.MATDES.2011.03.011

Tavakkolizadeh, M., and Saadatmanesh, H. (2001). Galvanic corrosion of carbon and steel in aggressive environments. *J. Compos. Constr.* 5 (3), 200–210. doi:10.1061/(ASCE)1090-0268(2001)5:3(200)

Twite, R. L., and Bierwagen, G. P. (1998). Review of alternatives to chromate for corrosion protection of aluminum aerospace alloys. *Prog. Org. Coatings* 33 (2), 91–100. doi:10.1016/S0300-9440(98)00015-0

Vakili, H., Ramezanzadeh, B., and Amini, R. (2015). The corrosion performance and adhesion properties of the epoxy coating applied on the steel substrates treated by cerium-based conversion coatings. *Corros. Sci.* 94, 466–475. doi:10.1016/J.CORSCI.2015.02.028

Vermeeren, C. A. J. R. (1991). *The application of carbon fibres in ARALL laminates*. Faculty of Aerospace Engineering, Report LR-658 [Preprint]. Delft University of Technology. Available at: https://repository.tudelft.nl/islandora/object/uuid%3Ae14663a0-6fe6-499d-b5dd-22e56ac8f127 (Accessed June 25, 2023).

Vinayagamoorthy, R., Manoj, I. V., Chand, I., Sai Charan, G. V., and Kumar, K. A. (2018). A central composite design based fuzzy logic for optimization of drilling parameters on natural fiber reinforced composite. *J Mech. Sci. Tech.* 32. doi:10.1007/s12206-018-0409-0

Vogelesang, L. B., and Vlot, A. (2000). Development of fibre metal laminates for advanced aerospace structures. *J. Mater. Process. Technol.* 103 (1), 1–5. doi:10.1016/S0924-0136(00)00411-8

Wang, W. X., Takao, Y., and Matsubara, T. (2007). Galvanic corrosion-resistant carbon fiber metal laminates. Available at: https://kyushu-u.elsevierpure.com/en/publications/galvanic-corrosion-resistant-carbon-fiber-metal-laminates (Accessed June 25, 2023).

Wang, X., Zhao, H., Wu, S., Suo, X., Wei, X., and Li, H. (2020). Aluminum-polyethylene composite coatings with self-sealing induced anti-corrosion performances. *J. Mater. Process. Technol.* 282, 116642. doi:10.1016/J.JMATPROTEC.2020.116642

Wu, G., and Yang, J. M. (2005). The mechanical behavior of GLARE laminates for aircraft structures. *JOM* 57 (1), 72–79. doi:10.1007/s11837-005-0067-4

Wu, G., Wang, X., Wu, Z., Dong, Z., and Zhang, G. (2014). Durability of basalt fibers and composites in corrosive environments. *J. Compos. Mater.* 49 (7), 873–887. doi:10.1177/0021998314526628

Wu, X., Zhan, L. h., Huang, M. h., Zhao, X., Wang, X., and Zhao, G. q. (2021). Corrosion damage evolution and mechanical properties of carbon fiber reinforced aluminum laminate. *J. Central South Univ.* 28 (3), 657–668. doi:10.1007/s11771-021-4635-8

Zhang, G. A., and Cheng, Y. F. (2009). Corrosion of X65 steel in CO2-saturated oilfield formation water in the absence and presence of acetic acid. *Corros. Sci.* 51 (8), 1589–1595. doi:10.1016/J.CORSCI.2009.04.004